Scanning Tunneling Microscopy

Graham Baker, Oğuzhan Can, and Étienne Lantagne-Hurtubise
(Dated: November 26, 2016)

We present the basics of the Scanning Tunneling Microscopy (STM) technique, along with some recent applications to research on quantum materials.

I. INTRODUCTION

A Scanning Tunneling Microscope (STM) is an instrument used to image and study the electronic properties of surfaces at the atomic scale. It was pioneered by Binnig, Röhrer and their groups in the early 1980s[1], earning them half of the 1986 Nobel Prize in Physics.

In an STM, an atomically sharp conducting tip is brought very close to the surface of the sample under study – the distance d between the two is on the order of a nanometer. The space between the tip and the sample, which is usually vacuum, forms a potential barrier. When a bias voltage V is applied between the tip and the sample, a tunneling current I_t flows between the two. The tunneling current depends on the tip-to-sample distance $d(\boldsymbol{r}) = z - z_0(\boldsymbol{r})$ where $z_0(\boldsymbol{r})$ is the profile of the sample's surface. It also depends on the local density of states (LDOS) of the sample over the energies within eV of the Fermi energy. STM is thus a powerful experimental technique for measuring the surface topography and LDOS of materials.

The following report is divided as follows: in Sec. II, we present the different data acquisition modes used with an STM, while Sec. III addresses some common experimental considerations. In Sec. IV, we explain the theory of electronic tunneling in the context of STM, and Sec. V concludes by presenting modern applications of STM in quantum materials.

II. MODES OF OPERATION

Figure 1 shows a schematic diagram of the experimental apparatus. Piezoelectric transducers are used to control the lateral position $\boldsymbol{r} = (x, y)$ of the tip as well as its height z. The piezoelectric transducer controlling height is also connected to a feedback control unit which depends on the tunneling current I_t. Usually, the tip is grounded and the bias voltage is the voltage $-V_s$ applied to the sample ($V_s > 0$ in the following, without loss of generality). Not shown in Figure 1 is the cryostat, which is used to cool the experiment.

Therefore, there are four (non-independent) tunable parameters during measurement: the tip height z, the tip position $\boldsymbol{r} = (x, y)$, the bias voltage $-V_s$, and the tunneling current I_t. Through controlling this set of parameters, one can operate a STM in several different modes: topography, spectroscopy and spectroscopic imaging[2]. In Figure 2, we show a representative example of a data set taken in each of these modes.

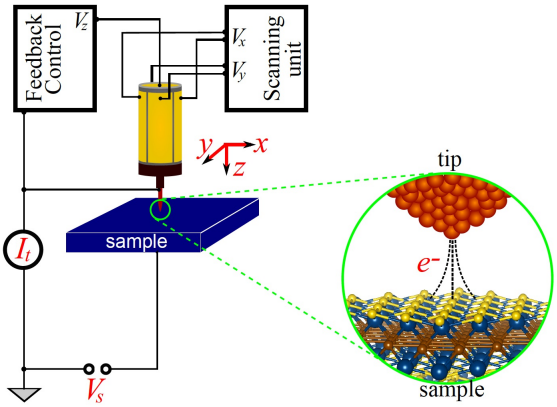

Figure 1. Schematic diagram of an STM. Figure taken from Ref. 3.

A. Topography

The first way in which an STM is used is to measure the topography of a sample's surface. There are two ways in which this can be done. In both cases, the sample voltage $-V_s$ is kept constant.

In constant current mode, the tip is scanned across the surface of the sample and the height z of the tip is controlled by a feedback loop in such a way as to maintain a constant tunneling current I_t. In this case, the height of the tip $z(\boldsymbol{r}) = z_0(\boldsymbol{r}) + d$ records the profile $z_0(\boldsymbol{r})$ of the sample's surface which contains the corrugations of the atomic lattice.

In constant height mode the tip is again scanned across the surface of the sample, this time at a constant height z, and the tunneling current $I_t(\boldsymbol{r})$ is measured at each position. Using the dependence of the current on the tip-to-sample distance $d(\boldsymbol{r}) = z - z_0(r)$, $I_t(\boldsymbol{r})$ can be used to deduce the surface profile $z_0(\boldsymbol{r})$ of the sample.

B. Spectroscopy

Scanning Tunneling Spectroscopy (STS) measures the electronic LDOS of the sample, by exploiting the fact that

$$\frac{dI_t}{dV_s} = C(d) \times \rho_s(\boldsymbol{r}, \epsilon = E_F - eV_s) \tag{1}$$

where $C(d)$ is an exponential function of the tip-sample distance d, as shown in Sec. IV. Therefore, the LDOS

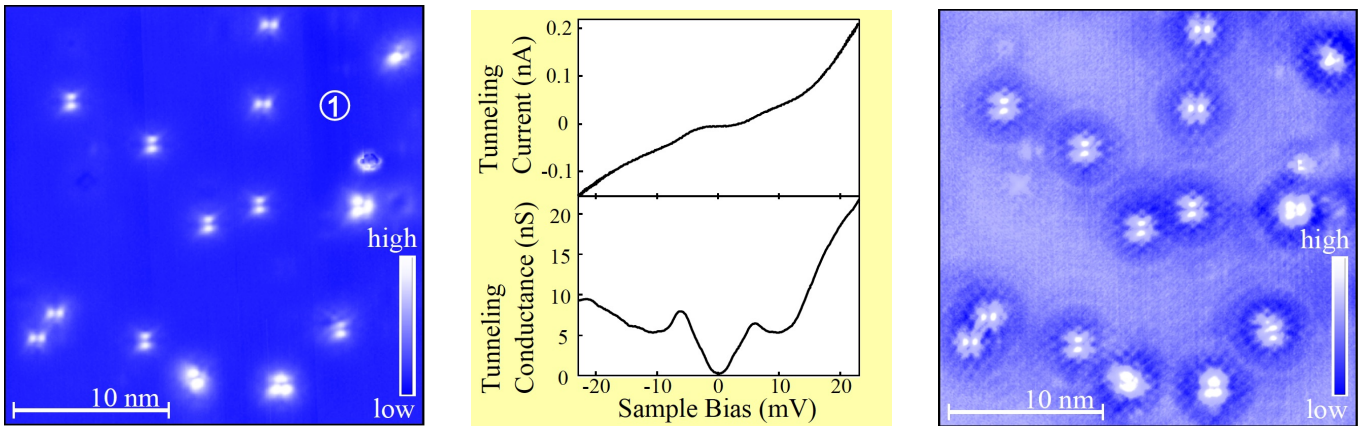

Figure 2. Left: Topographic image of LiFeAs with impurities in bright contrast. Center: STS taken at location indicated by 1 in left panel. Right: Tunneling conductance map measured over same area as in left panel. Figure taken from Ref. 3.

can be measured by keeping the tip at a constant height and position and measuring the tunneling conductance dI_t/dV_s while sweeping V_s. There are two ways of measuring dI_t/dV_s.

The first way is to measure $I_t - V_s$ data and perform numerical differentiation. This technique offers a high data acquisition rate however the process of numerical differentiation introduces noise to the measurement. The second method is to use a lock-in amplifier to modulate V_s by a small voltage $V_s^{AC}\sin(\omega t)$. Using the condition that $V_s^{AC} \ll V_s^{DC}$ and expanding I_t in series one finds that

$$I_t = I_t^{DC} + \frac{dI_t}{dV_s} V_s^{AC}\sin(\omega t) + \mathcal{O}\left(\left(V_s^{AC}\right)^2\right) \qquad (2)$$

so that the signal at ω is proportional to dI_t/dV_s[4,5]. This technique can improve measurement sensitivity if ω is selected so that it is far from the frequencies of sources of noise. However, the time constant of the lock-in amplifier is on the order of 10 milliseconds, which when repeated for each data point can significantly decrease the data acquisition rate.

C. Spectroscopic Imaging

In Spectroscopic Imaging STM (SI-STM) the topography and STS modes are combined. As in the topographic mode of operation, the tip is scanned across the sample's surface at constant V_s while either d or I_t is held constant and the variation in the other is recorded. This time, at each pixel in the topographic map the tip freezes its position $(z, \boldsymbol{r})$ and sweeps V_s while measuring dI_t/dV_s. By plotting dI_t/dV_s at a given V_s as a function of lateral position $\boldsymbol{r}$, the spatial variation of the LDOS is mapped.

III. EXPERIMENTAL CONSIDERATIONS

A. Temperature

The lower the temperature at which STM measurements are performed, the better the resolution. This is because as temperature decreases, so does the thermal broadening of the Fermi-Dirac distribution. The lower limit to energy resolution due to thermal broadening is given by $\Delta E_{\text{thermal}} = \frac{7}{2}k_B T$ where k_B is Boltzmann's constant[6]. Typically, STMs are cooled by helium which, depending on the pressure and which isotope is used, gives access to temperatures from 300 mK to 4.2 K. By using a dilution refrigerator, temperatures below 300 mK can be accessed. With the push to examine phenomena that occur at ever smaller energy scales, the design and realization of dilution refrigerator STMs has been the source of much recent experimental effort[6–8].

B. Vibration Isolation

Because of the exponential dependence of the tunneling current on the tip-to-sample distance d, STMs are extremely sensitive to the effects of vibrations, which can be significant sources of noise in measurements. Vibration isolation is thus a critical consideration in STM experimental design. Since the corrugation of an atomically flat sample surface can be as low as 10 pm, it is commonly concluded that d should change no more than 1 pm due to the influence of vibrations[2,9,10]. Vibration isolation takes place at multiple stages of the STM apparatus: at the STM head (which contains the tip and sample), between the head and the cryostat, and between the entire apparatus and the external environment.

STM heads are designed to be extremely rigid so that, when exposed to vibrations, the tip and sample move together and the tip-to-sample distance d is preserved.

For helium temperature STMs, the head is mounted

within the cryostat by eddy-current-damped spring suspensions to achieve vibration isolation. However, in dilution refrigerator STMs, the spring suspensions form too poor a thermal link between the refrigerator and the head. To operate at such low temperatures, it is necessary to compromise on the vibration isolation that can be achieved at this stage of the apparatus.

For high-performance STM experiments, extensive effort goes into the design of ultra-low vibration facilities. In a typical facility of this type, the STM is mounted on a pneumatically suspended inertia block weighing on the order of $10^3 - 10^4$ kg. The entire experiment is housed in an acoustically-absorbing enclosure, and rests on foundation which is isolated from that of the rest of the building[11].

IV. THEORY

A. Tunneling current and DOS

In this section, we derive how the LDOS is related to the tunneling current measured by an STM.

Applying a bias voltage $-V_s$ to the sample (while the tip is grounded) shifts the energy of the electrons in the sample by $+eV_s$ with respect to the electrons in the tip, as shown in Figure 3. Tunneling can occur through the vacuum in between the tip and the sample – the tunneling *current* measured will be $I = -e\Gamma$, where Γ is the transition rate (probability of transitioning from initial to final state per unit time). Using time-dependent perturbation theory (Fermi's golden rule), the tunneling currents are found to be:

$$I_{sample\to tip} = -2e\frac{2\pi}{\hbar}|M(\epsilon)|^2 n(\epsilon)\rho_s(\mathbf{r},\epsilon) \times [1-n(\epsilon+eV_s)]\,\rho_t(\epsilon+eV_s) \quad (3)$$

and

$$I_{tip\to sample} = -2e\frac{2\pi}{\hbar}|M(\epsilon)|^2 n(\epsilon+eV_s)\rho_t(\epsilon+eV_s) \times [1-n(\epsilon)]\,\rho_s(\mathbf{r},\epsilon) \quad (4)$$

where the factor of 2 in front accounts for spin, $M(\epsilon)$ is the matrix element of the tunneling process, which in general depends on the energy, $\rho_s(\mathbf{r},\epsilon)$ and $\rho_t(\epsilon)$ are the local electronic density of states (LDOS) of the sample and the tip, respectively, and

$$n(\epsilon) = \frac{1}{e^{\beta(\epsilon-E_F)}+1}$$

is the fermion number density in a state of energy ϵ, E_F is the Fermi energy and $\beta \equiv 1/k_BT$ is the inverse temperature. The fermion number densities in Eqs. (3) and (4) appear because tunneling can only occur if the initial state is occupied and the final state is empty. The net tunneling current I_t is comprised of the current from the sample to the tip, minus the current from the tip to the sample, integrated over all energies:

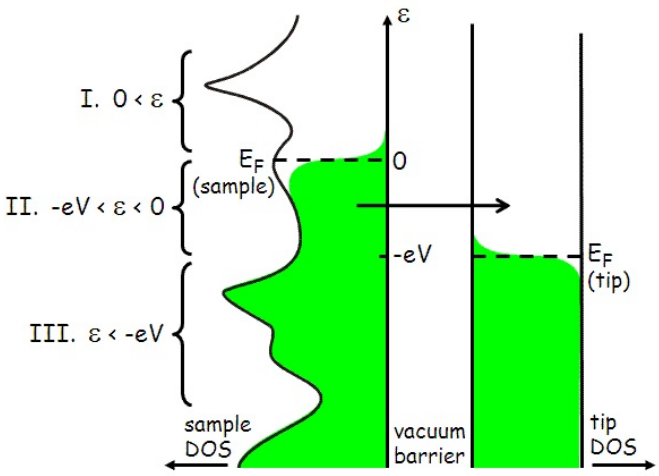

Figure 3. Density of states (DOS) as a function of energy for a generic STM sample (left) and tip (right). When a bias voltage $-V$ is applied, the Fermi energy of the tip is shifted by $-eV$ with respect to the Fermi energy E_F of the sample. The green regions represent occupied states at low temperatures, and the solid arrow shows the main tunneling channel from the sample to the tip. Figure taken from Ref. 12

$$I_t = -\frac{4\pi e}{\hbar}\int_0^\infty d\epsilon |M(\epsilon)|^2 \rho_s(\mathbf{r},\epsilon)\rho_t(\epsilon+eV_s) \times\{n(\epsilon)\,[1-n(\epsilon+eV_s)] - n(\epsilon+eV_s)\,[1-n(\epsilon)]\} \quad (5)$$

where we have taken the lowest electronic eigenstate to lie at $\epsilon = 0$. At low temperatures, the Fermi-Dirac distribution is very sharp, so we can suppose that states in the sample are filled up to $\epsilon = E_F$ and states in the tip are filled up to $E_F - eV_s$. In that setting, electrons in the tip have nowhere to tunnel through (all states in the sample with corresponding energy are already occupied), whereas sample electrons with energy in the range $[E_F - eV_s, E_F]$ can tunnel to the tip and contribute to the integral. Furthermore, in order to extract information on the DOS of the sample electrons, we choose a tip made of a material with a constant DOS over the range of energies of interest. Thus, the integral simplifies to:

$$I_t = -\frac{4\pi e}{\hbar}\rho_t(E_F)\int_{E_F-eV_s}^{E_F} d\epsilon |M(\epsilon)|^2 \rho_s(\mathbf{r},\epsilon) \quad . \quad (6)$$

The last step is to figure out the matrix element for the process. A useful approximation in this case is to model the potential barrier as a square well with height ϕ and width d (the sample-tip distance). The tunneling through such a potential can be estimated using the WKB method[13], leading to $|M|^2 = e^{-2\gamma}$, where

$$\gamma = \frac{d}{h}\sqrt{2m\phi}$$

which is independent of the energy of the electron, so that

$$I_t(\mathbf{r}, V_s) = -\frac{4\pi e}{\hbar}\rho_t(E_F)e^{-d\sqrt{8m\phi}/h}\int_{E_F-eV_s}^{E_F} d\epsilon\rho_s(\mathbf{r},\epsilon) \quad . \tag{7}$$

The total tunneling current is proportional, under our present assumptions, to the integral of the sample electronic DOS on the interval $[E_F - eV_s, E_F]$. Therefore,

$$\rho_s(\mathbf{r}, \epsilon = E_F - eV_s) \propto \frac{dI_t(\mathbf{r}, V_s)}{dV_s} \quad . \tag{8}$$

B. Quasiparticle Interference

Impurities on the surface of a material lead to Friedel oscillations. These are oscillations in the electronic density of states at the surface, caused by the scattering and interference of the electronic surface states on the impurities. Therefore, Friedel oscillations can be seen in STM images as oscillations in the local density of states near the Fermi level[14]. This modulation pattern in the local density of states is referred to as quasiparticle interference, and contains information about the wave vectors connecting surface electronic states near the Fermi level. The Fourier Transform of a tunneling conductance map gives us the Fermi contour in momentum space because the modulation waves in LDOS are composed of surface state wave vectors near the Fermi level. Figure 4 is an example of the surface state of Be(0001), which is a good candidate for the experimental realization of a free electron gas[14].

In the figure, we see the tunneling conductance map (a) and its Fourier Transform (b). As we expect from a free electron gas, the Fermi contour can be seen as a circle. This technique allows us to study the surface states in both real and reciprocal space. However, ARPES can only access occupied states and cannot obtain real space information. With STM, LDOS oscillations in real space observed through tunneling conductance maps allow us to delve deeper into understanding disorder and scattering processes on material surfaces.

The electronic properties of surfaces are crucial for the investigation of materials such as topological materials and high temperature superconductors.

V. MODERN APPLICATIONS OF STM

A. Topological Materials

Topological insulators are materials with a gap in the bulk and symmetry protected gapless states on the surface which can be described by a massless Dirac Fermion Hamiltonian. In the presence of certain symmetries, as long as the gap in the bulk does not close, the topological insulator phase is robust against disorder. With their peculiar surface states, topological materials have promising applications ranging from spintronics to quantum computation.

One of the hallmark features of these surface states is the absence of scattering between states of opposite spin and momentum (see Ref. 16 and 17 for a comprehensive review).

In Ref. 18, the authors used STM – combined with ARPES – to image the gapless surface states of compound $Bi_{1-x}Sb_x$, and probe the scattering of the edge states on defects created by random alloying. They show that back-scattering is absent even for strong atomic-scale disorder, a result consistent with the theory of 3D topological insulators. Around the same time, another group reported similar conclusions by applying STM to the topological insulator Bi_2Te_3[19].

Weyl semimetals are another kind of topological material with interesting surface properties (see Ref. 20 for an introduction). A peculiar property of the surface states of Weyl semimetals are the Fermi arcs. Fermi arcs are Fermi contours that are not closed loops and can only exist on the surface as a boundary of a 3D material. Weyl semimetals have also been investigated using STM with QPI methods[21]. Although Fermi arcs are not directly observable on the momentum space QPI images, signatures of Fermi arcs can be identified[22]. It is an important milestone that evidence for Fermi arcs has been shown for the first time independently from and agreeing with ARPES results.

B. Vortices on Superconductors

STM has been an important tool in probing superconductors. For instance, the superconducting gap can be observed by tunneling spectroscopy if we plot LDOS versus bias $-V_s$ (See Figure 5 – bottom curve) The gap is where the LDOS vanishes. STM has also played an important role in the experimental verification of Abrikosov vortices.

Abrikosov vortices are topological defects that occur in type-II superconductors when an external magnetic field above a critical value is applied (in fact, they are the defining property for this phase). In this regime, the magnetic field pierces through the superconductor instead of being expelled by it. Each vortex has a magnetic flux quantum Φ_0 and these vortices can form lattices (Figure 4.c) that are accessible to an STM[15]. The electronic structure of these vortices and their spatial distribution provide insight into fundamental properties of the superconducting state. For example, the size of the vortex states can be used to measure the superconducting coherence length[23].

STM studies not only allowed the experimental observation of these vortices with high spatial resolution, but also played a crucial role in exploring them further. The superconducting gap closes at these vortices which show no superconducting behaviour. It was expected

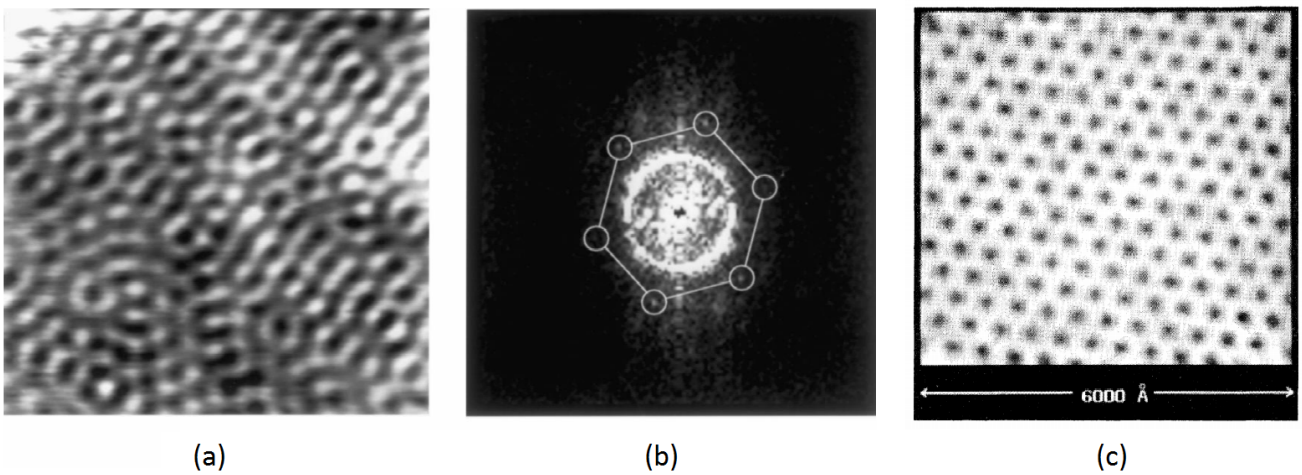

Figure 4. (a) Tunneling conductance map of Be(0001) showing LDOS oscillations in real space. (b) Fourier Transform of (a). Figures taken from Ref. 14. (c) Topographic image of an Abrikosov vortex lattice on the surface of $NbSe_2$. Figure taken from Ref. 15

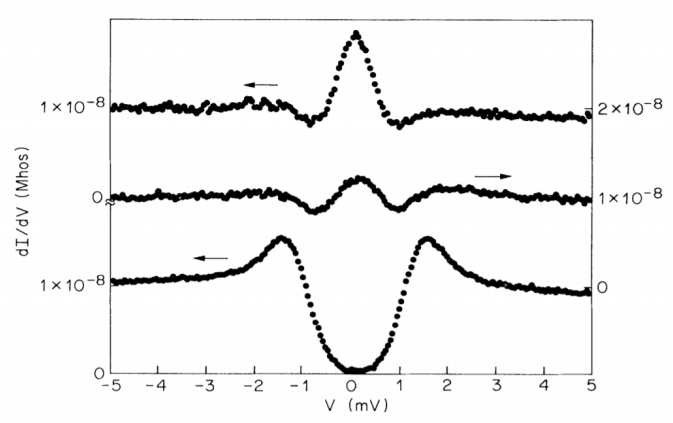

Figure 5. Density of states vs bias voltage for $NbSe_2$ near an Abrikosov vortex. Three measurements were made for different distances from the vortex: the core center (top), 75 Å from the vortex (middle) and far away from a vortex (bottom). Note the superconducting gap at zero bias voltage in the bottom curve. Figure from Ref. 15.

that these vortices would be metallic since the superconducting gap is closed and there are states in place of the gap for electrons to tunnel into. Therefore, the superconducting gap would not be seen, instead the observed conductance versus bias voltage would be a flat signal when the tip goes through the vortex. However, instead of a flat spectrum Hess et al. found a peak[15] at the zero bias voltage (Figure 5), indicating the existence of localized vortex core states. This discovery lead to further interest in the study of Abrikosov lattices.

VI. CONCLUSION

Scanning Tunneling Microscopy is a powerful experimental technique that has allowed to investigate the surface electronic states of a large array of materials with atomic resolution. It is likely that it will play a pivotal role in the research and development of the next generation of quantum materials.

[1] G. Binnig, H. Rohrer, C. Gerber, and E. Weibel, Phys. Rev. Lett. **49**, 57 (1982).
[2] C. J. Chen, *Introduction to scanning tunneling microscopy*, Vol. 2 (Oxford University Press New York, 2005).
[3] S. Chi, *Scanning Tunneling Microscopy Study of Superconducting Pairing Symmetry: Application to LiFeAs*, Ph.D. thesis, The University of British Columbia (2014).
[4] O. Fischer, M. Kugler, I. Maggio-Aprile, C. Berthod, and C. Renner, Rev. Mod. Phys. **79**, 353 (2007).
[5] J. Tersoff and D. R. Hamann, Phys. Rev. Lett. **50**, 1998 (1983).
[6] M. Assig, M. Etzkorn, A. Enders, W. Stiepany, C. R. Ast, and K. Kern, Rev. Sci. Instrum. **84**, 033903 (2013).
[7] U. R. Singh, M. Enayat, S. C. White, and P. Wahl, Rev. Sci. Instrum. **84**, 013708 (2013).
[8] Y. J. Song, A. F. Otte, V. Shvarts, Z. Zhao, Y. Kuk, S. R. Blankenship, A. Band, F. M. Hess, and J. A. Stroscio, Rev. Sci. Instrum. **81**, 121101 (2010).
[9] M. Okano, K. Kajimura, S. Wakiyama, F. Sakai, W. Mizutani, and M. Ono, Journal of Vacuum Science & Technology A **5** (1987).
[10] D. W. Pohl, IBM J. Res. Dev. **30**, 417 (1986).
[11] B. Macleod, *An Ultra-Low-Vibration Facility for Housing a Dilution Temperature Scanning Tunneling Microscope*, Master's thesis, The University of British Columbia (2015).

[12] Z. Zhu and Y. He, "Hoffman lab website - scanning tunneling microscopy," .
[13] D. J. Griffiths, *Introduction to Quantum Mechanics, 2nd edition* (Pearson Education, 2005).
[14] L. Petersen, P. Hofmann, E. Plummer, and F. Besenbacher, J. Electron. Spectrosc. Relat. Phenom. **109**, 97 (2000).
[15] H. F. Hess, R. B. Robinson, R. C. Dynes, J. M. Valles, and J. V. Waszczak, Phys. Rev. Lett. **62**, 214 (1989).
[16] M. Z. Hasan and C. L. Kane, Rev. Mod. Phys. **82**, 3045 (2010).
[17] X. L. Qi and S. C. Zhang, Rev. Mod. Phys. **83** (2011).
[18] P. Roushan, J. Seo, C. V. Parker, Y. S. Hor, D. Hsieh, D. Qian, A. Richardella, M. Z. Hasan, R. J. Cava, and A. Yazdani, Nature **460**, 1106 (2009).
[19] T. Zhang, P. Cheng, X. Chen, J. F. Jia, X. Ma, K. He, L. Wang, H. Zhang, X. Dai, Z. Fang, X. Xie, and Q. K. Xue, Phys. Rev. Lett. **103**, 1 (2009).
[20] X. Wan, A. M. Turner, A. Vishwanath, and S. Y. Savrasov, Phys. Rev. B **83**, 205101 (2011).
[21] H. Zheng, S.-Y. Xu, G. Bian, C. Guo, G. Chang, D. S. Sanchez, I. Belopolski, C.-C. Lee, S.-M. Huang, X. Zhang, R. Sankar, N. Alidoust, T.-R. Chang, F. Wu, T. Neupert, F. Chou, H.-T. Jeng, N. Yao, A. Bansil, S. Jia, H. Lin, and M. Z. Hasan, .
[22] G. Chang, S.-Y. Xu, H. Zheng, C.-C. Lee, S.-M. Huang, I. Belopolski, D. S. Sanchez, G. Bian, N. Alidoust, T.-R. Chang, C.-H. Hsu, H.-T. Jeng, A. Bansil, H. Lin, and M. Z. Hasan, Phys. Rev. Lett. **116**, 066601.
[23] J. E. Hoffman, Rep. Prog. Phys. **74**, 124513 (2011).